Atmos. Chem. Phys. Discuss., 8, 14819–14839, 2008
www.atmos-chem-phys-discuss.net/8/14819/2008/

Atmospheric Chemistry and Physics Discussions

This discussion paper is/has been under review for the journal *Atmospheric Chemistry and Physics (ACP)*. Please refer to the corresponding final paper in *ACP* if available.

Detection of ship tracks in ATSR2 satellite imagery

E. Campmany[1], R. G. Grainger[1], and S. M. Dean[2]

[1]Atmospheric, Oceanic and Planetary Physics, University of Oxford, Oxford, UK
[2]National Institute of Water and Atmospheric Research Ltd, Wellington, New Zealand

Received: 30 May 2008 – Accepted: 2 July 2008 – Published: 1 August 2008

Correspondence to: E. Campmany (campmany@atm.ox.ac.uk)

Published by Copernicus Publications on behalf of the European Geosciences Union.

Abstract

Ships modify cloud microphysics by adding cloud condensation nuclei (CCN) to a developing or existing cloud. These create lines of larger reflectance in cloud fields that are observed in satellite imagery. Ship tracks are most frequently seen off the west coast of California, and the Atlantic coast of both west Africa and south-western Europe. In order to automate their detection within the Along Track Scanning Radiometer 2 (ATSR2) data set an algorithm was developed and integrated with the Global Retrieval of ATSR Cloud Parameters and Evaluation (GRAPE) processing chain. The algorithm firstly identifies intensity ridgelets in clouds which have the potential to be part of a ship track. This identification is done by comparing each pixel with its surrounding ones. If the intensity of three adjacent pixels is greater than the intensity of its neighbours, then it is classified as a ridgelet. These ridgelets are then connected together, according to a set of connectivity rules, to form tracks which are classed as ship tracks if they are long enough. The algorithm has been applied to two years of ATSR2 data. A month of results have been compared with other satellite datasets to validate the algorithm. There is a high ratio of false detections. Nevertheless the global distribution of ship tracks shows a similar pattern to the ship emissions distribution.

1 ATSR2 and GRAPE

The Along Track Scanning Radiometer (ATSR2) is on board a low Earth orbit satellite at a height of about 780 km, performing approximately 14 orbits in one Earth day (Mutlow, 1999). The instrument is capable of receiving information from both a forward and nadir view of width of about 500 km. In the case of the nadir view, used in this study, it has a scan swath of 575 pixels in width, with a nominal pixel size of 1 km by 1km at the centre of the swath. This leads to every point on the Earth's surface being mapped nominally 10 times a month. The channels in which radiance is measured are 0.55 μm, 0.67 μm, 0.87 μm, 1.6 μm, 3.7 μm, 10.8 μm, 12 μm (referred to as channels 1 to 7 respectively).

ACPD

8, 14819–14839, 2008

The Global Retrieval of ATSR Cloud Parameters and Evaluation (GRAPE) project has produced a global cloud and aerosol data set from the entire ATSR2 dataset (1995–2001 at present). Version 2 of the dataset has now been produced, with much improved accuracy over version 1, and is accessible (with registration) from the British Atmospheric Data Centre (BADC). The analysis has been performed using the Oxford/RAL Aerosol and Cloud (ORAC) optimal estimation retrieval scheme. The dataset includes the following parameters on an orbit by orbit basis (at the 3×4 km resolution) and as 2.5° resolution monthly means (along with error estimates for each value): Cloud fraction, cloud phase (water or ice), cloud top temperature, cloud top pressure, cloud top height, cloud optical depth (at 0.55 μm), cloud effective radius, cloud liquid water path, skin temperature, aerosol optical depth (at 0.55 μm), aerosol effective radius and surface albedo at 0.55 μm. Validation of cloud and aerosol properties derived using the GRAPE algorithm is ongoing (Thomas et al., 2007; Campmany et al., 2007). The algorithm has been applied to the GRAPE Level2 products with a resolution of 3×4 km.

1.1 Ship tracks formation

Clouds are a suspension of small water droplets. A small droplet of pure water is likely to evaporate unless it is above a critical radius, at which point it becomes stable, and from which it can continue to grow by condensation. The change in Gibbs free energy in the formation of a spherical droplet of radius a is given by

$$\Delta G = -\frac{4}{3}\pi a^3 \rho_l RT \ln\left(\frac{e}{e_s(T)}\right) + 4\pi a^2 \gamma, \quad (1)$$

where ρ_l is the density of the liquid, R is the gas constant, T is the temperature, e is the partial pressure, e_s is the saturated vapour pressure and γ is the surface tension (Andrews, 2000). The first term on the right side of the equation is known as the "bulk" term, and the second the 'surface' term. It is easy to see that a critical radius, a_c, exists

ACPD
8, 14819–14839, 2008

when ΔG is a maximum, $\frac{d\Delta G}{da}=0$

$$a_c = \frac{2\gamma}{\rho_l RT \ln\left(\frac{e}{e_s}\right)}. \quad (2)$$

A droplet with radius above the critical radius can form by homogeneous nucleation of water molecules, but the probability of this happening is tiny. Most cloud water droplets are formed as a result of a soluble particle acting as a CCN. The presence of a CCN increases the size of the bulk term in Eq. (1) making it more energetically favourable for water molecules to grow to the size of the critical radius. The size of the critical radius is reduced when CCN are present and the number of water droplets increases (Erlick et al., 2001).

Sea salt is a common naturally occurring CCN, but anthropogenic aerosols are also very effective (Taylor, 2005). The sulphates released in ship stack emissions act as very efficient CCN, hence the formation of ship tracks.

It is hypothesised that certain background environmental conditions need to be in place before the formation of ship tracks can occur (Durkee et al., 2000a). These conditions include a small boundary layer depth, pre-existing cloud formation mechanisms, and CCN concentration below a threshold value. The Monterey Area Ship Track (MAST) study returned average values of wind speed of 7.8 ms^{-1}, surface pressure of 1018.3 mb and surface temperature of 287.8 K (Durkee et al., 2000b)

1.2 Properties and effects

The properties of ship tracks vary widely and they have been investigated by various studies: Coakley et al. (1987); Albrecht (1989); Platnick and Twomey (1994); Ferek et al. (1998); Coakley and Walsh (2002); Schreier et al. (2006). The most extensive of these was MAST which combined in situ measurements with satellite imagery from the Advanced Very High Resolution Radiometer (AVHRR). The MAST experiment studied

ACPD
8, 14819–14839, 2008

ship tracks for one month off the coast of California. The results gained from the analysis of 131 ship tracks produced by known ships showed that the average ship tracks had length 296±233 km and width 9±5 km (Durkee et al., 2000b). Ship tracks are rarely found in cloud at an altitude above 1 km (Coakley et al., 2000). Thus ship tracks have the potential to cover a relatively large area and this indicates that their effects could have a large effect on the Earth's climate, if ship tracks are found to have a frequency of occurrence which is globally significant. The results of the MAST experiment showed that ship tracks have a wide range of optical properties. The contrast between the optical properties of ship tracks and those of unpolluted background cloud was also shown to vary. The average ambient cloud reflectance in AVHRR 3.7 μm channel was 11±4 % while the ship track reflectance at the same wavelength was 14 ± 5 %. The difference in optical properties varied not only between ship tracks but also along the lengths of individual tracks on a scale of 1 km to 25 km. The MAST results showed a significant difference in all the examined properties of ship tracks. This makes the development of a method of automated detection very difficult. Without an exact definition of a ship track it is hard to invent a method of selecting them from an image, especially when a ship track is embedded within background cloud.

The optical depth of a cloud of water droplets, in which the water droplets are large compared to the wavelength of incident light, is given by

$$\tau = 2\pi h N \bar{r}^2, \tag{3}$$

where h is the cloud depth, N is the number density of the droplets and $\bar{r}$ is the mean droplet radius (Twomey et al., 1966). The number density of droplets, N, can be approximated by

$$N \propto \frac{\text{water content of cloud}}{\text{volume of a droplet}} \propto \frac{1}{\bar{r}^3} \tag{4}$$

hence,

$$\tau \propto \frac{1}{\bar{r}}. \tag{5}$$

ACPD
8, 14819–14839, 2008

Differences in 0.3–3.0 μm albedo and transmission between the clouds and ship tracks as a result of the changes in drop size distribution and composition were found by Erlick et al. (2001). In this study the ship tracks presence caused the absorption of infrared radiation to rise from 39.0 Wm^{-2} to 45.5 Wm^{-2}, and the reflectivity from 0.361 to 0.673. On a large scale, these figures could potentially have a very significant affect on the world's climate.

Albrecht (1989) proposed one further effect ship tracks could have on cloud cover, and hence the climate: a reduction in drizzle. An increase in CCN concentrations, as already seen, reduces the size of cloud droplets. This in turn decreases the probability of cloud droplets colliding and hence growing to the size required for them to fall as precipitation. The ultimate effect of this is to increase the lifetime of clouds, further increasing the albedo of ship tracks.

2 Algorithm description

The problem of ship track detection is similar to the contrail (condensation trail) detection problem since both are formed as a result of the increase in CCN. However contrails form as cirrus cloud in the upper atmosphere. There are several existing methods to detect contrails, based on straight line detection using Hough transforms relying on the fact that jet aircraft mainly fly in straight lines at speed suficient that they create linear ridges in the image. However, straight line detection is less appropiate in the case of ship tracks, which are formed over longer scales. The age of a ship track is 7.3±6.0 h (Durkee et al., 2000b), a timescale which allows for significant distorsion by dispersion and geostrophic effects. It is therefore unsurprising that less work has been done on the automated detection of ship tracks.

ACPD
8, 14819–14839, 2008

2.1 Filters

The algorithm firstly identifies intensity ridgelets in clouds which have the potential to be part of a ship track. This identification is done by comparing each pixel with its surrounding ones. If the intensity of three adjacent pixels is greater than the intensity of its neighbours, then it is classified as a ridgelet. These ridgelets are then connected together, according to a set of connectivity rules, to form tracks (the continuation of the track is allowed in the co-linear, parallel or 45 degrees direction), and finally are classed as ship tracks if they are long enough. In order to apply the algorithm to potential scenes of ship tracks, some preprocessing screening is required by using different filters.

The information from 12 μm channel data, stored as brightness temperature, is used by the algorithm as an initial filter. This is done by comparison to a data set of calculated clear sky brightness temperatures produced by RTTOV, an algorithm run by ECMWF reanalysis (European Centre for Medium-range Weather Forecasting). This data product is produced by including actual observations of the temperature and humidity profiles of the atmosphere as input to the model, which is then used to 'fill in' the rest for unobserved regions. Since the tracks only occur at low altitude the brightness temperature of tracks seen by the satellite will be close to that of the surface. The rate of change of temperature with height (the atmospheric lapse rate) close to the Earth's surface is about 6.5 K km^{-1} (Stephens, 1994). Given that the tracks form in the boundary layer, mostly well below 1 km, and rounding up to allow for diurnal temperature variation and errors, this can be used to set a maximum temperature difference above the surface layer of 10 K. Using these criteria it can be determined whether or not pixels show cloud low enough to be ship tracks, and thus eliminating those pixels in which the cloud is above the boundary layer.

In 1.6 μm channel images, cloud-covered areas show up as areas of higher intensity compared to the clear areas seen near the coastline. It is therefore reasonable to set a lower limit on the intensity of pixels which are to be considered. In the algorithm this is

ACPD
8, 14819–14839, 2008

done by setting a parameter for the lower limit, relative to the median pixel intensity for the orbit from which the image is taken. This serves as a means by which some noise arising from pixels with no cloud or insufficient cloud can be removed. By using exactly the median value it can be said that half the pixels will be automatically discounted.

2.2 Ridge detection

Initially pixels are analysed individually in relation to the pixels surrounding them to determine whether or not they could be part of a ridge segment in any of four orientations. These are the vertical, horizontal and two diagonals with respect to the image.

The pixel's intensity is analysed relative to comparison pixels at a specified spacing in the appropriate direction to determine whether or not its intensity is greater; the geometry of this is shown in Fig. 1a,b. Here the situation is one with a comparison pixel either side at a pixel spacing of two. The use of one pixel either side was envisaged but the algorithm allows for a second to be specified.

The analysis leads to four arrays of information, one for each orientation, to specify which pixels have met the criteria to potentially form part of a ridgelet (line segment) in the corresponding directions.

The 1.6 μm channel intensity, as a continuous variable input, will satisfy the ridge pixel criteria quite often even for relatively featureless areas of cloud. It is therefore useful to define a minimum intensity difference between the test pixel and the comparison pixels that must be exceeded in order to make the classification. In the code this was set with reference to the median pixel intensity for initial trials but this could easily be hard coded, or given as a declared variable that is specified when executing the code.

2.2.1 Ridgelet definition

Ridgelets are defined by the algorithm as three adjacent pixels, satisfying the criteria in Sect. 2.2 for a given direction, in a row in the correct sense as shown for a horizontal

ACPD
8, 14819–14839, 2008

ridgelet in Fig. 1c. By scanning the image for such groupings this refined information can be stored in four arrays (one for each orientation). This was done by recording the centre pixel of each such 1×3 pixel rideglet in the array for the appropriate orientation. This gives a method of approximating image structure, which may not be straight, to a series of straight line segments. It also retains the information about the sense in which they are orientated.

2.3 Track classification

With rideglets defined from a filtered set of pixels the algorithm has a basis from which to find longer sections of ridge. The method used consists of a set of connectivity rules: from each ridgelet pixel the surrounding pixels are examined to determine whether or not any other ridgelet pixels are located such that they may reasonably form part of the same ridge. If an appropriate ridgelet exists the algorithm then traces along to it and searches for more ridgelets according to the same set of rules.

Allowed continuation ridgelets for the tracing are shown in Fig. 2. With 4 (1×3 pixel) ridgelet types defined this leads to 8 different track end situations to be accounted for in the connectivity rules, i.e. for each ridgelet the track could be being followed by the code in one of two (opposite) directions. The general rule applied was that part of a ridge could turn by up to 45 degrees in the image between ridgelets. It was also deemed acceptable that gaps could be jumped when tracing ridges, provided the ridge segment continued in a straight line along the image from the previous ridgelet. Figure 2 shows this for a horizontal ridgelet and a diagonal one; rotations of these apply for the other six track directions.

The algorithm traces a track until it reaches a dead end, this being where it cannot find another ridgelet to which it can connect. Up to this point the path taken from the start pixel is recorded so that at the end of the trace it can be decided whether or not to retain the track. In theory the best criteron in deciding whether or not to retain a trace, and mark an area as ship track, is length. This could be done on pixel count, but to speed computation it was based on loops through the connectivity rules. This

ACPD
8, 14819–14839, 2008

gives a higher weighting for a continuing straight line segment than one with the same number of pixels which changes in direction. This is because when tracing along a straight line the jump between ridgelet centres for each loop is only one pixel, hence increasing the number of pixels in the track by 1 for each loop rather than 2 or 3, as can be seen in Fig. 2. However, since tracks are generally locally straight this was seen as no disadvantage.

3 Algorithm aplication

3.1 Validation

Because the algorithm is completely automatic a validation by eye is needed. A subset of one month has been used to study the false detections and the possible real tracks missed by the detector, comparing the ATSR2 images with Moderate Resolution Imaging Spectroradiometer (MODIS) satellite data. Four hundred and nineteen ATSR2 orbits were analyzed and compared with the corresponding false-colour MODIS image at the closest time for April of 2000. Of these 419 orbits, 101 presented ship tracks detected by the automated algorithm and after comparing with MODIS, only 8 were real, mostly located in the North Pacific ocean (west of California). Also, 3 real ship tracks were spotted in the MODIS images which the detector has failed to detect. The algorithm detects lots of long-scale fronts and other cloud patterns that have features similar to the ship tracks as shown in Fig. 4, even after filtering the images to only look at low-level cloud. The validation shows that the algorithm is far from being perfect but it gives a fraction of the recognised features that are really ship tracks. Hence we can apply it as is, and use our validation to normalise the estimated number of tracks.

3.2 Statistic Analysis

The algorithm has been applied to two years of ATSR2 data (1999 and 2000). In total, 4360 orbits were analyzed and 1924 ship tracks were detected, including false

ACPD
8, 14819–14839, 2008

detections. Figure 4 shows an example of a ship track detected. The scene is from 25th February 2000 and ships tracks can be clearly seen in a MODIS satellite image of the area, taken on the same day. The image, which is a false colour composite based on three channels, shows a large number of tracks, in a region of cloud, off the coast of California. On the left an image of the ATSR2 1.6 μm channel taken at aproximately the same time, and at the bottom the result of applying the algorithm.

In order to visualize the global distribution of ship tracks, the coordinates of the detected tracks have been plotted in Fig. 5 for both years. As can be appreciated in the figure, most of the tracks are located in the North Pacific and Atlantic oceans, while in the Southern Hemisphere there are hardly any tracks. There are no main differences between different years. The plots look quite similar to the global distribution of NO_x emissions from ships presented by Eyring et al. (2005) (Fig. 6) even though the plots show all the detections performed by the algorithm, including the false positives. There are also previous studies of global distribution of ship tracks from satellite imagery that obtain very similar results (Schreier et al., 2007).

The results can also be presented distributed by latitude and by month to study the seasonal and latitudinal patterns (Fig. 7). The seasonal variation is strong in both years showing a maximum in summer. The annual distribution of relative area of ship tracks shows similar pattern as well, with a maximum area of 4×10^{-3} % ($4\times10^{5} km^2$). The area is calculated computing all the pixels marked as a track and the relative ratio is determined by dividing by the total area of the orbit. The values showed at Fig. 7 correspond to data integrated for the whole day. It is worth noticing that the seasonal distribution of vessel traffic, extracted from Corbett et al. (2007), hardly presents a seasonal cycle. The latitudinal distribution shows a larger number of occurrencies for latitudes between 30 and 60 North. Compared with the vessel traffic data given by Endresen et al. (2005), it can be apreciated that the pattern is roughly the same.

ACPD
8, 14819–14839, 2008

4 Conclusions

An algorithm to detect ship tracks has been described and applied. Initially the algorithm identifies intensity ridgelets in clouds which have the potential to be part of a ship track. These ridgelets are then connected together, according to a set of connectivity rules, to form tracks and are finally classed as ship tracks if they are long enough. The algorithm has been applied to two years of ATSR data by processing 4360 orbits. One thousand nine hundred and twenty four tracks were detected, including false detections, showing a global distribution similar to the ship emissions distribution with a maximum occurrence in the north Pacific and Atlantic. A subset of the results has been compared with MODIS images showing a large number of false detections (90% of the cases), however these false positives cannot be considered a random noise since their distribution shows a resemblance to the ship emissions distribution. An improvement of the algorithm could be implemented in a future by using the microphysical properties retrieved by the GRAPE algorithm as new conditions for the detection of ship tracks.

Acknowledgements. The authors would like to thank Daniel White for his help in developing and coding the algorithm. This work has been supported by the QUANTIFY project which is funded by the European Commission within the 6th research framework programme.

References

Albrecht, B. A.: Aerosols, cloud microphysics and fractional cloudiness, Science, 245, 1227–1230, 1989. 14822, 14824

Andrews, D. G.: An Introduction to Atmospheric Physics, chap. 3, Cambridge University Press, 55–90, 2000. 14821

Campmany, E., Thomas, G., Carboni, E., Poulsen, C., Grainger, R., Lawrence, B., and Watts, P.: Initial results from the GRAPE version 2 aerosol and cloud climatology, in: Geopys. Res. Abstr., 9, p. 04376, 2007. 14821

Coakley, J. A. and Walsh, C. D.: Limits to the aerosol indirect radiative effect derived from observations of ship tracks, J. Atmos. Sci., 59, 668–680, 2002. 14822

Coakley, J. A., Bernstein, R. L., and Durkee, P. A.: Effect of ship-stack effluents on cloud reflectivity, Science, 237, 1020–1022, 1987. 14822

Coakley, J. A., Durkee, P., Nielsen, Taylor, J., Platnick, S., Albrecht, B., Babb, D., Chang, F., Tahnk, W., Bretherton, C., and Hobbs, P.: The Appearance and Disappearance of Ship Tracks on Large Spatial Scales, J. Atmos. Sci., 57, 2765–2778, 2000. 14823

Corbett, J. J., Wang, C., Winebrake, J., and Green, E.: Allocation and Forecasting of Global Ship Emissions, Tech. rep., Clean Air Task Force, Boston, MA, USA, 2007. 14829

Durkee, P. A., Noone, K. J., and Bluth, R. T.: The Monterey Area Ship Track Experiment, J. Atmos. Sci., 57, 2523–2541, 2000a. 14822

Durkee, P. A., Chartier, R., Brown, A., Trehubenko, E., Rogerson, S., Skupniewicz, C., Nielsen, K., Platnick, S., and King, M.: Composite Ship Track Characteristics, J. Atmos. Sci., 57, 2542–2553, 2000b. 14822, 14823, 14824

Endresen, Sigrid, E., Sundet, J. K., Dalsiren, S. B., Isaksen, I. S., Berglen, T. F., and Gravir, G.: Emission from international sea transportation and environmental impact, J. Geophys. Res., 108, D174560, doi:10.1029/2002JD002898, 2005. 14829

Erlick, C., Russell, L. M., and Ramaswamy, V.: A microphysics-based investigation of the radiative effects of aerosol-cloud interactions for two MAST Experiment case studies, Geophys. Res. Atmos., 106, 1249–1269, 2001. 14822, 14824

Eyring, V., Kohler, H. W., Aardenne, J., and Lauer, A.: Emissions from international shipping, J. Geophys. Res., 110, D17305, doi:10.1029/2004JD005619, 2005. 14829

Ferek, R. J., Hegg, D. A., Hobbs, P. V., Durkee, P., and Nielsen, K.: Measurements of ship-induced tracks in clouds off the Washington coast, J. Geophys. Res., 206, 23 199–23 206, 1998. 14822

Mutlow, C.: ATSR-1/2 User Guide, 1.0 edn., 29 pp., 1999. 14820

Platnick, S. and Twomey, S.: Determining the Susceptibility of Cloud Albedo to Changes in Droplet Concentration with the Advanced Very High Resolution Radiometer, J. Appl. Meteorol., 33, 334–347, 1994. 14822

Schreier, M., Mannstein, H., Eyring, V., and Bovensmann, H.: Global ship track distribution and radiative forcing from 1 year of AATSR data, Geophys. Res. Lett., 34, L17814, doi:10.1029/2007GL030664, 2007. 14829

Schreier, M., Kokhanovsky, A. A., Eyring, V., et al.: Impact of ship emissions on the microphysical, optical and radiative properties of marine stratus: a case study, Atmos. Chem. Phys., 6, 4925–4942, 2006,

http://www.atmos-chem-phys.net/6/4925/2006/. 14822
Stephens, G. L.: Remote Sensing of the Lower Atmosphere, chap. 1, Oxford, University Press, 3–33, 1994. 14825
Taylor, F.: Elementary climate physics, Oxford University Press, 232 pp., 2005. 14822
Thomas, G. E., Poulsen, C. A., Curier, R. L., Lewuw, G., Marsh, S. H., Carboni, E., Grainger, R. G., and Siddans, R.: Comparison of AATSR and SEVIRI aerosol retrievals over the Northern Adriatic, Q. J. Roy. Meteorol. Soc., 133, 85–95, 2007. 14821
Twomey, S., Jacobowitz, H., and Howell, H. B.: Comments on Anomalous cloud lines, J. Atmos. Sci., 23, 101–108, 1966. 14823

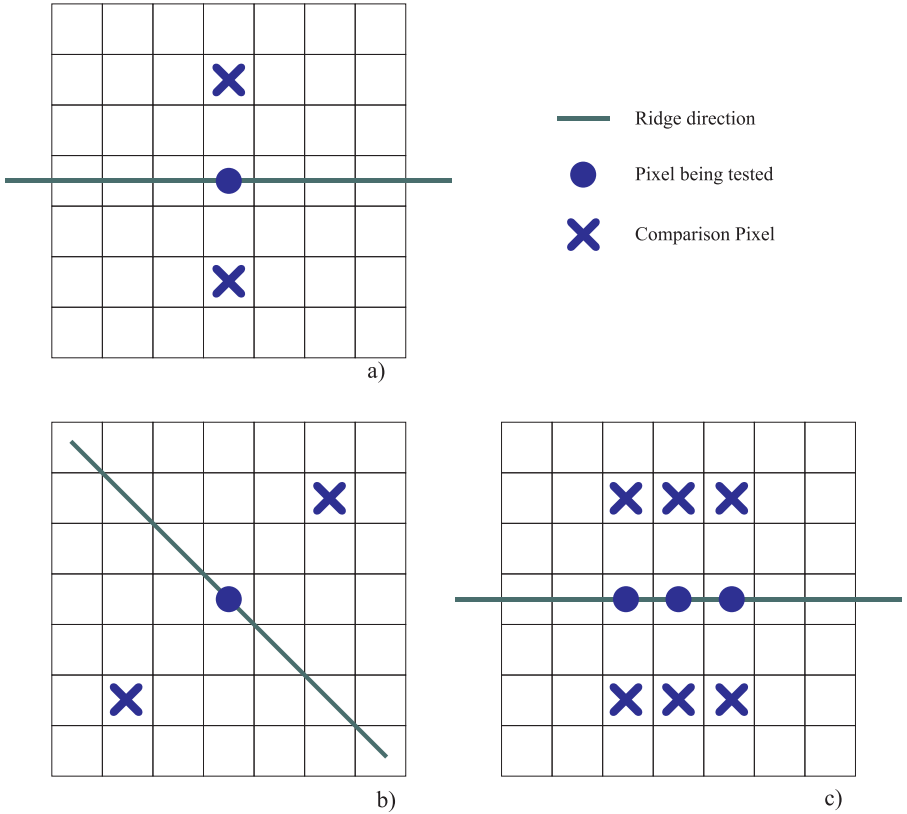

Fig. 1. Pixel orientation test for: **(a)** horizontal alignment, **(b)** a diagonal alignment. The net test geometry for a horizontal ridgelet is shown in **(c)**. The comparison pixels must be less intense than the corresponding test pixel for classification to be made.

ACPD
8, 14819–14839, 2008

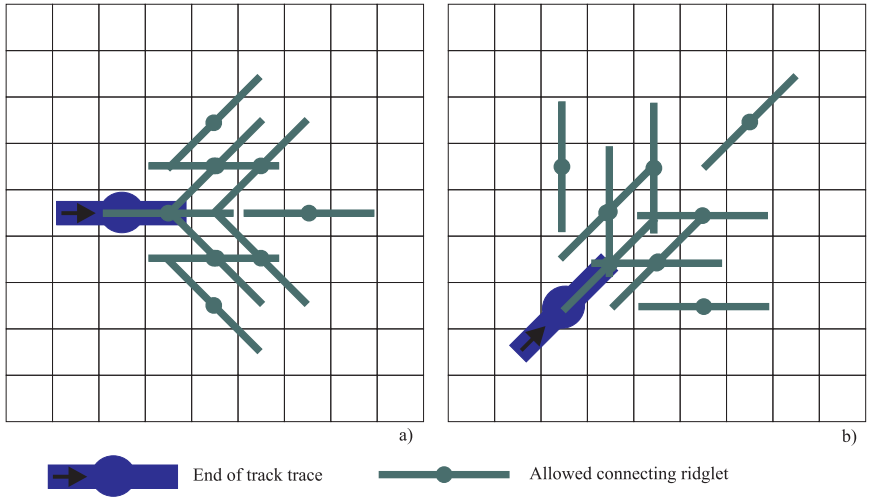

Fig. 2. The connectivity rules for progressing the trace of a track. **(a)** shows this for a horizontal segment tracing from the left, **(b)** shows this for a diagonal segment coming up from the left.

ACPD
8, 14819–14839, 2008

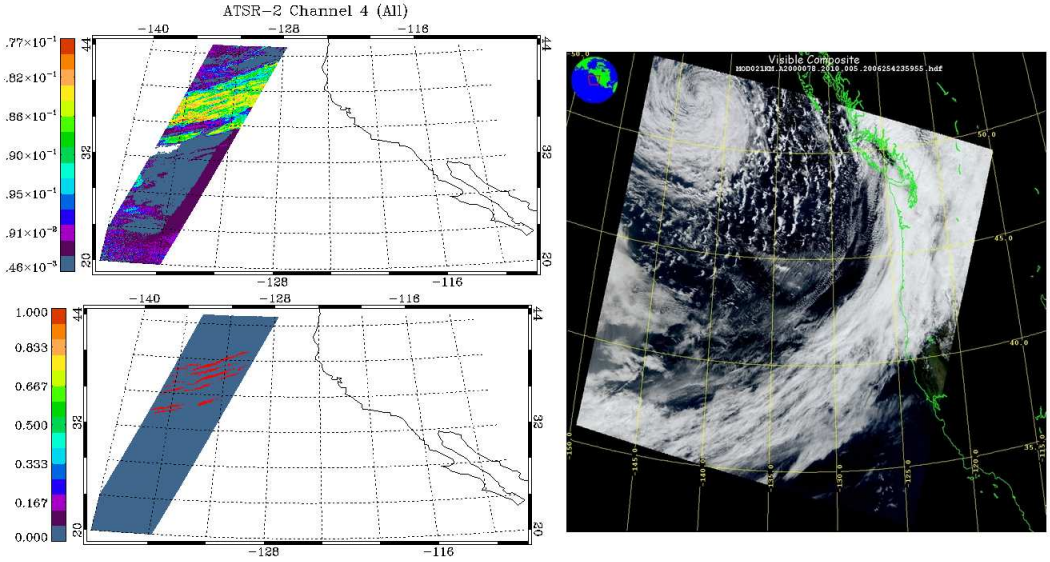

Fig. 3. Example of a false detection performed by the algorithm. The scene corresponds to 18th March 2000, off the coast of California. Top-left: ATSR2 1.6μm channel. Bottom-left: Ship track mask detected. Right: MODIS image false colour.

ACPD
8, 14819–14839, 2008

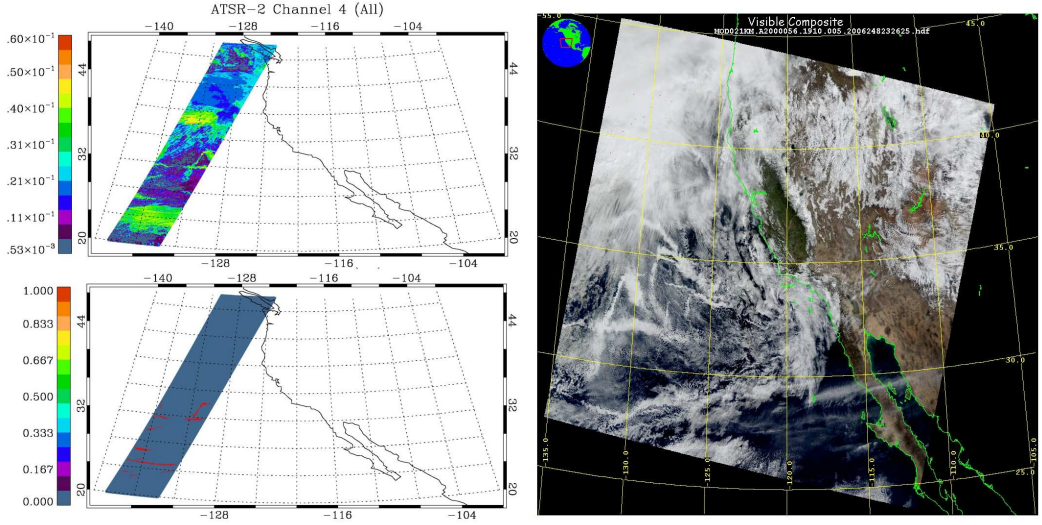

Fig. 4. Example of scene with ship tracks on 25th February 2000, off the coast California. Top-left: ATSR2 1.6μm channel. Bottom-left: Ship track mask detected. Right: MODIS image false colour.

ACPD
8, 14819–14839, 2008

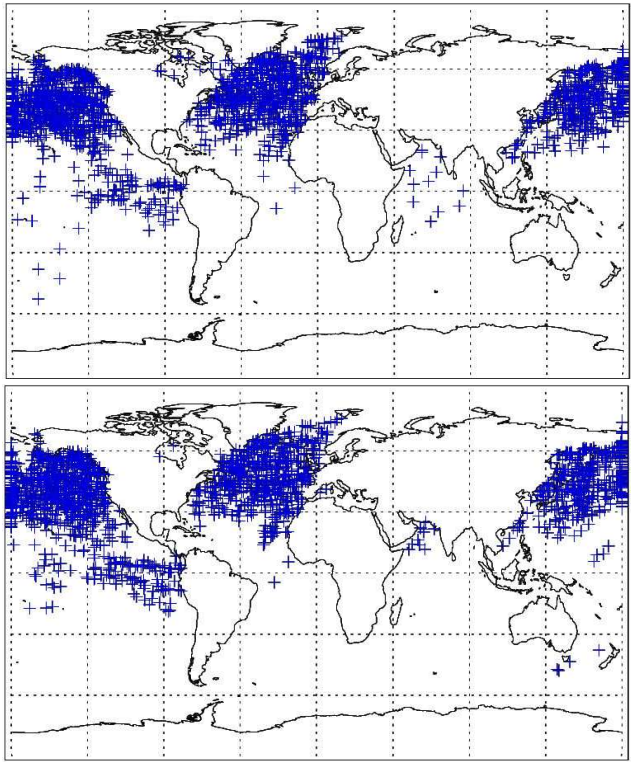

Fig. 5. Global distribution of ship tracks as detected with the algorithm of ATSR2 images for the years 1999 (top) and 2000 (bottom).

ACPD

8, 14819–14839, 2008

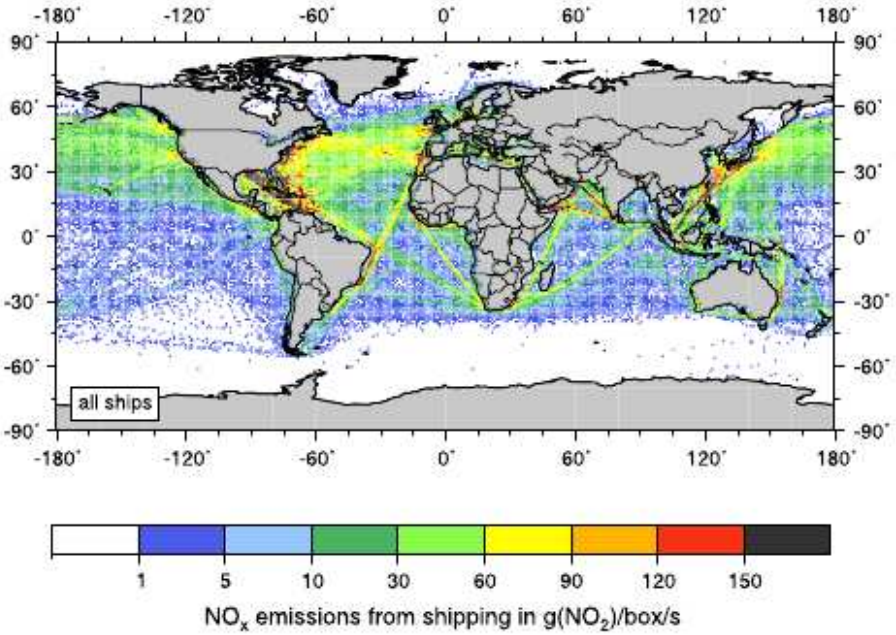

Fig. 6. Global distribution of NO_x emissions for different ship types (adapted from Eyring et al., 2005).

ACPD
8, 14819–14839, 2008

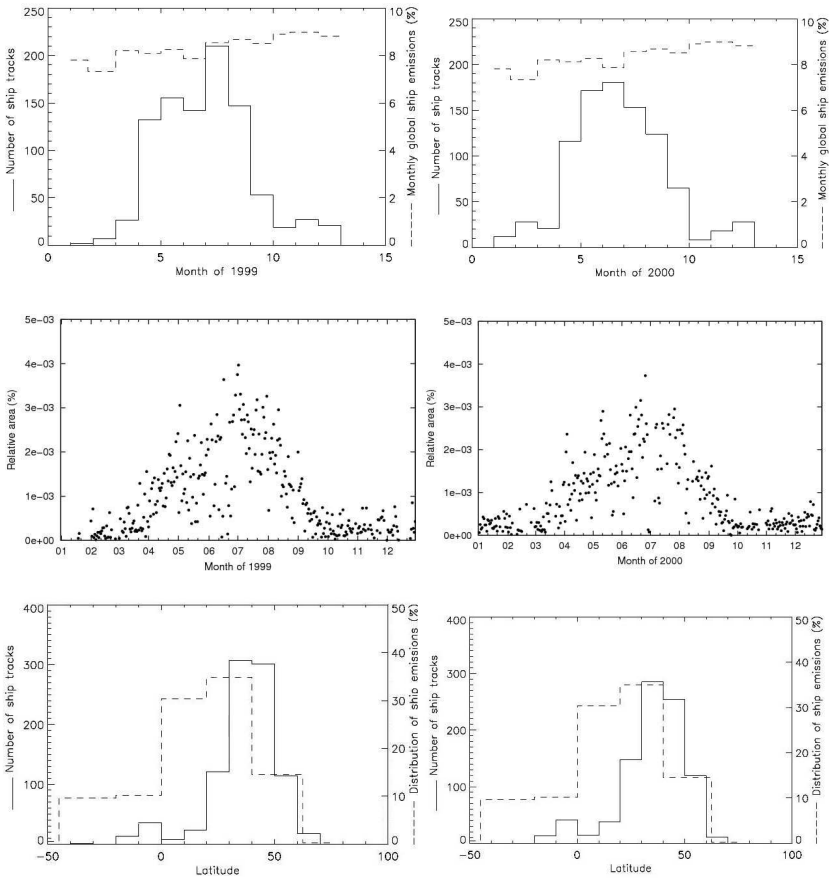

Fig. 7. Monthly (top) and latitudinal (bottom) distribution of ship tracks compared with vessel traffic for 1999 (left) and 2000 (right). The relative area of ship tracks distributed by month is also shown (centre).

ACPD
8, 14819–14839, 2008